A Preliminary Design Tool for Hollow Cathodes

IEPC-2017-328

Presented at the 35th International Electric Propulsion Conference
Georgia Institute of Technology • Atlanta, Georgia • USA
October 8 – 12, 2017

M. Panelli[1], A. Smoraldi[2] and F. Battista[3]
C.I.R.A., Italian Aerospace Research Center, Capua (CE), 81043, Italy

Abstract: This paper presents a preliminary design tool for orificed hollow cathodes. Two physical models compose the tool: a plasma model and a thermal model. A time-independent, volume-averaged model has been developed to determine plasma properties in the emitter and orifice regions. A Lumped Element Thermal Model has been also developed to compute temperature distributions and the respective gradients within the main cathode's element. The study, conducted to validate the results of the models, shows that there is a good agreement with values and trends found in the available literature. The tool is able to estimate performances of new devices by the calculation of cathode working conditions for different geometries given device operating condition and insert material.

Nomenclature

A_{eff}	=	offective emission area
d_o	=	orifice diameter
I_d	=	discharge current
j	=	total current density
j_i	=	ion current density
J	=	radiosity
$j_{i,o}$	=	ion current density in the orifice region
j_{th}	=	ion thermal flux
j_{em}	=	thermionic current density
j_{er}	=	thermal flux of electrons recombining on the insert wall
k_B	=	Boltzmann constant
K_i	=	ionization rate coefficient
Kn	=	Knudsen Number
K_l	=	coefficient of loss through orifice entrance
LETherM	=	CIRA Lumped Elements Thermal Model
LSVC	=	Large Scale Vacuum Chamber
L_o	=	orifice length
L_{eff}	=	effective emission length
$\dot{m}$	=	mass flow-rate
m_e	=	electron mass
m_i	=	ion mass
MSVC	=	Medium Scale Vacuum Chamber
n or n_e	=	electron number density
$n_{e,e}$	=	electron number density in the emitter region

[1] Researcher, Methodologies and Technologies for Space Propulsion, m.panelli@cira.it.
[2] Researcher, Propulsion Test Facilities, a.smoraldi@cira.it.
[3] Head of Methodologies and Technologies for Space Propulsion, f.battista@cira.it.

$n_{e,o}$ = electron number density in the orifice region
n_0 = neutral number density
$n_{0,e}$ = neutral number density in the emitter region
$n_{0,o}$ = neutral number density in the orifice region
$\dot{n}_{ion}$ = ion loss rate
$\dot{n}_{out}$ = volumetric ion production rate
P_{ion} = energy losses due to neutral-particle ionization
P_{cont} = pressure computed for a continuum flow
P_{conv} = energy losses due to electron convection
P_{er} = loss due to the electrons recombining on the emitter surface
P_{em} = power gained by the emitted electrons
P_{ds} = ion losses across the double sheath
P_{in} = external power input at thermal node i
P_{kin} = pressure computed from the kinetic theory of gases
P_R = resistive heating due to the Joule effect
P_i = power removed by the ions leaving the control volume
$P_{i,o}$ = power delivered to the plasma by the ions arriving from the orifice
P_o = sonic pressure at the orifice exit
q = electron elementary charge
r_o = orifice radius
r_e = emitter internal radius
R = plasma resistance
R_i = equivalent radiation resistance
$R_{i,j}$ = equivalent radiation resistance between node i,j
$R_{cond\ ij}$ = equivalent conduction resistance
R_g = gas constant
T_e = electron temperature
$T_{w,o}$ = temperature of the orifice wall
T_s = temperature of emitter wall
T_i = temperature at node i
T_j = temperature at node j
V_p = emitter sheath voltage drop
V_{ds} = voltage drop across a planar double sheath

α = degree of ionization
γ = ratio of specific heats
$\langle\varepsilon_i\rangle$ = average energy losses due to a single ionization event
η = plasma resistivity
$\langle\sigma_{en}\rangle$ = electron-neutral effective collision cross section
σ_{SB} = Stefan-Boltzmann constant
$\bar{u}_o$ = average velocity in the orifice
μ = dynamic viscosity
ν = collision frequency
ν_{en} = collision frequency between electron and neutral
ν_{ei} = collision frequency between electron and ion

I. Introduction

ELECTRIC propulsion is a technology aimed at achieving thrust with high exhaust velocities, which results in a reduction in the amount of propellant required for a given space mission or application compared to other conventional propulsion methods. Reduced propellant mass can significantly decrease the launch mass of a spacecraft or satellite, leading to lower costs from the use of smaller launch vehicles to deliver a desired mass into a given orbit or to a deep-space target. In general, electric propulsion (EP) encompasses any propulsion technology in which electricity is used to increase the propellant exhaust velocity. Presently, Electric Propulsion systems are proposed for a large class of primary propulsion applications, such as high altitude orbit raising, orbit transfer and high impulse interplanetary scientific missions, allowing to lower the cost of commercial and institutional satellites and to enable missions which have requirements hardly to be fulfilled by other propulsion system.

In this frame, with PRORA funds, CIRA implemented an Electric Propulsion Program, called IMP-EP, with the goal to enable technical and testing capabilities for national and international EP developments. This program is structured in three main lines: I. design and realization of two facilities (MSVC, LSVC) including the improvement of test definition and competences. II. Development and improvement of basic and advanced diagnostics methodologies. III. Development of design methodologies and technologies for electrical thrusters, including the set-up of a preliminary design tool, improvement of numerical modeling along with post-test analyses and laboratory models manufacturing.

In the frame of line III the development, of a low power Hall thruster, to be tested in the MSVC facility, is currently ongoing. In order to design the cathode for this thruster, and to develop models for electric propulsion, a preliminary numerical design tool, describing the physics of orificed hollow cathode (OHC) devices with low work function insert, has been developed, combining relevant literature models.

Two sub modules compose the tool: a plasma model and a thermal model. Plasma model includes a current density equation, ion flux balances, plasma power balances and plasma pressure equations. Two systems of equations, one for the emitter region and one for the orifice region, are solved to compute the averaged plasma number densities, the electron temperatures, the neutral number densities and the overall cathode voltage drop. The routine employs the fsolve MatLAB® routine with dedicated graphical user interface (GUI); a convergence check is performed at each iteration by comparing the evolution of the relative error until the stop condition is met.

The heat transfer mechanisms and the related temperature gradients along the cathode are evaluated with the aid of an in-house Lumped Element Thermal Model (LETherM), which accounts for temperature-dependent material properties.

After a brief description of the models, the paper reports the results of the validation phase, where plasma models and thermal model have been separately tested. The results of the simulations have been compared with the available experimental/numerical data and trends found in the literature on existing devices, showing good agreement.

The coupling between plasma and thermal model, useful to update orifice and emitter wall temperatures, is currently in progress.

The tool is able to estimate quickly the performances of new devices by the calculation of cathode working conditions (temperatures, voltages, number densities) for different geometries given device operating condition (propellant, discharge current and mass flow rate) and materials.

II. Cathode architecture

Ion and Hall thrusters that utilize an electron discharge to ionize the propellant gas and create the plasma in the thruster require a cathode to emit the electrons. In addition, thrusters must neutralize the ion beam leaving the thruster by providing electrons emitted from a cathode into the beam[1]. Due to its high performances in terms of lifetime (~10^4 hours), the most used configuration is that of OHC.

A sketch of a typical OHC configuration is shown in Figure 1. A neutral gas (e.g. Xenon, Krypton) flows in a conductive refractory metal tube. A low-work function material namely insert is located within the main tube and it is electrically connected to it. The insert material acts as electron-emitter providing high emission current densities (~10^6 Am^{-2}) with low plasma potentials, typically less than 20 V [4]. Rare-earth emitters, (e.g. Lanthanum or Cesium Hexaboride) provide a superior resistance to contaminants along with a reduced evaporation respect to a refractory-metal porous matrix filled with an emissive compound. However, rare-earth emitters react with many refractory metals at high temperature, so a very thin graphite shield is often need to be between the emitter and the main tube.

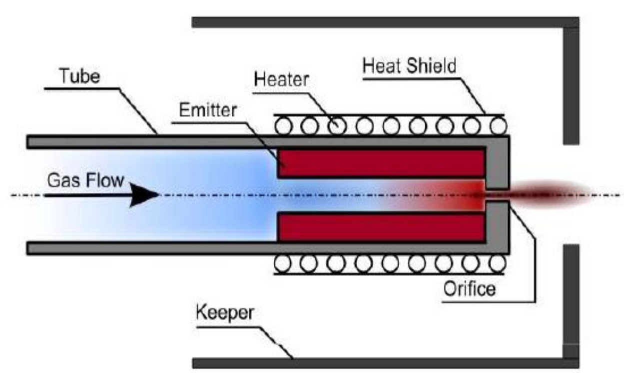

Figure 1. Schematic of typical orificed hollow chatode[2].

An orifice plate at the tube exit maintains a relatively high internal pressure, typically p∼10^3 -10^4 Pa. The high pressure results in a low plasma potential, which, in turn, increases the ionization efficiency and reduces the energy of the ions reaching the cathode walls. This also prevents erosion of the structure, enhancing lifetime.

The keeper electrode is an outer tube that helps turning on the cathode by applying a positive potential with respect to the inner tube and protects the cathode interior parts from high-energy ion bombardment, enhancing lifetime, too. The emitter-material is usually heated up to the thermionic emission temperatures by an external source; this element namely heater is typically a resistive element in physical contact with the tube external surface.

A thermal shield wraps the outer of the heater filament in order to reduce the overall power consumption.

III. Model Overview

The model presented in this work is composed by two main parts: in the first part, the orifice plasma module and the insert plasma module calculate the respective main plasma parameters; these modules use as input first guess wall temperatures (particularly, orifice and insert wall temperature), the geometry and the operative conditions of the cathode. Subsequently, the cathode thermal model updates the temperature profile, using the computed plasma power inputs (Figure 2).

The description of the plasma models and thermal model follows.

A. Plasma models

The model is time-independent, volume-averaged and can determine plasma properties within the two, coupled regions in which plasma has been ideally divided: the orifice and the insert (emitter) regions.

Three equations are solved to compute the plasma parameters in the orifice region. Particularly they are the number density, $n_{e,o}$, the electron temperature, $T_{e,o}$, and the neutrals density, $n_{0,o}$. Following the reliable literature, the equations are the ion flux conservation equation[5], internal plasma power equation[4,5] and pressure equation[4,6].

The emitter model includes four equations based on previous work. A current density equation[1,4], a ion conservation equation[4], a plasma power balance[1,4] and a plasma pressure equation[1,5] are used to compute plasma number density, $n_{e,e}$, the electron temperature, $T_{e,e}$, the neutrals density $n_{0,e}$, and the emitter sheath voltage drop V_p.

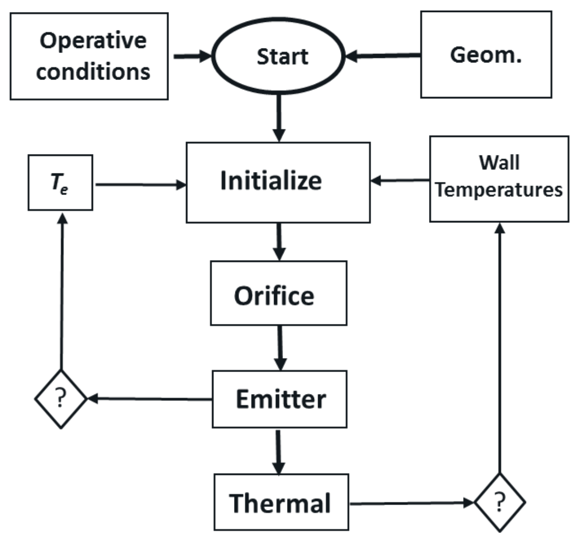

Figure 2. Flow Chart of the model.

All these quantities are obtained setting up the operating conditions (mass flow rate, $\dot{m}$ and discharge current, I_d), the main geometrical parameters (e.g. orifice diameter, d_o, cathode length, l_o), the constructive material properties (mainly insert and main tube) and the propellant (e.g. Xenon, Krypton). In this formulation, orifice and insert temperatures are also code input: the user must start with first guess temperature and changing it until the systems converge. In the present version of the code, the effective emission length is input parameter that has been found by means of semi-empirical approach.

After the model solution converges, several Knudsen numbers are calculated in the orifice and emitter regions to verify that the plasma is indeed collisional, and the Debye ratio and particle count in a Debye sphere are evaluated to determine if the ionized gas meets the conditions for a plasma.

B. Orifice Plasma model

1) *Ion Flux Balance*

In steady-state operation the ion loss rate, $\dot{n}_{\mathrm{out}}$, is balanced by the volumetric ion production rate, $\dot{n}_{\mathrm{ion}}$, Eq. (1), in the orifice plasma region:

$$\dot{n}_{ion} = \dot{n}_{out} \tag{1}$$

Hence, the ion balance conservation equates the creation of ions through electron-impact ionization and the flux of ions leaving orifice control volume (Figure 3), either through the sheath surrounding the orifice surfaces (assumed to include the orifice inlet) or through thermal efflux at the orifice outlet, towards the keeper and anode, as suggested by Eq. (2).

$$q\pi r_o^2 L_o n_{0,o} n_{e,o} K_i = j_{i,o}(2\pi r_o L_o + \pi r_o^2) + j_{th}\pi r_o^2 \qquad (2)$$

Where, j_i[5] is the ion current density calculated from the Bohm sheath criterion and j_{th}[5] is the ion thermal flux through the exit section. The ionization rate coefficient, K_i[1], is computed as a function of the electron temperature assuming a direct electron-impact ionization[1].

In the Eq. (2) the assumption that a double sheath exists at the constriction of the orifice entrance, preventing the flow of ions from the insert region, has been made.

Figure 3. Insert and Orifice control volumes.

2) Internal Power Balance

The plasma power balance states that the resistive heating, P_R, balances the energy losses due to neutral-particle ionization, P_{ion}, to the electron convection, P_{conv}, and to the ion losses across the double sheath, P_{ds}, namely:

$$P_R = P_{ion} + P_{conv} + P_{ds} \qquad (3)$$

$$RI_d^2 = \dot{n}_{ion}\langle\epsilon_i\rangle + \frac{5}{2}\frac{k_B}{q} I_d\left(T_{e,o} - T_{e,e}\right) + V_{ds} I_d \qquad (4)$$

$$R = \frac{\eta L_o}{\pi r_o^2}, \eta = \frac{\nu m_e}{n q^2} \qquad (5)$$

Where $\langle\epsilon_i\rangle$ is the average energy losses due to a single ionization event. The potential drop across the double sheath, V_{ds}, is evaluated by means of a planar approximation, Eq. (6) as reported in Ref. 7.

$$V_{ds} = \left(\frac{9 I_d k_B T_e}{7.5\pi r_o^2 n q^2}\sqrt{\frac{m_e}{2q}}\right)^{2/3} \qquad (6)$$

Excitation and radiation losses are neglected since the mean path for photon absorption is much lower than the orifice diameter.

The plasma resistance is evaluated using Eq. (5). The total collision frequency includes the contributions of electron-ion and electron-neutral collisions, namely

$$\nu = \nu_{ei} + \nu_{en} \qquad (7)$$

where the electron-ion collision frequency, ν_{ei}, is computed as a function of the Coulomb logarithm[8].

The resistance of the plasma is obtained with both electron-ion and electron-neutral collisions[8]. The electron-neutral collision cross-section is estimated from Eq. (9), while the collision frequency is estimated with the thermal velocity of the electrons, Eq. (8)**.**

$$\nu_{en} = \langle\sigma_{en}\rangle n_0 \left(\frac{k_B T_e}{n_e}\right) \qquad (8)$$

$$\langle\sigma_{en}\rangle = 6.6\cdot 10^{-19}\frac{\frac{T_e k_B}{4q} - 0.1}{1 + \left(\frac{T_e k_B}{4q}\right)^{1.6}} \qquad (9)$$

3) Pressure Equation

Even if a transitional model would be more appropriated, since typical Knudsen numbers (Kn) in the orifice range between 0.01 and 0.05 [4], the last equation, selected to close the orifice system, equates the plasma pressure, as computed from the kinetic theory of gases, with the pressure of a continuum flow, Eq. (10-11), assuming a sonic condition at the orifice exit section.

$$P_{kin} = P_{cont} \qquad (10)$$

$$\left(n_{e,o}+n_{0,o}\right)k_B T_{wo}\left(1+\frac{\alpha T_{e,o}}{T_{w,o}}\right)=\frac{\dot{m}}{\pi r_o^2}\sqrt{\frac{R_g T_{w,o}}{\gamma}\left(1+\frac{\alpha T_{e,o}}{T_{w,o}}\right)} \tag{11}$$

Where $T_{w,o}$ is the orifice wall temperature and α is the degree of ionization.

C. Insert Plasma model

1) Current Equation

Defining the effective emission area as $A_{eff} = \pi r_e^2 L_{eff}$ the current density equation can be expressed as:

$$j=\frac{I_d}{A_{eff}}=j_i+j_{em}-j_{er} \tag{12}$$

where j_i is the ion current density collected at the emitter surface as computed from the Bohm sheath criterion, j_{em} is the thermionic current density and j_{er} , Eq. (13), is the thermal flux of electrons recombining on the insert wall.

$$j_{er}=\mathrm{q}\frac{1}{4}\mathrm{n}exp\left(-\frac{qV_p}{k_B T_s}\right)\left(\frac{8k_B T_e}{\pi m_e}\right)^{1/2} \tag{13}$$

being V_p the emitter sheath voltage drop.

The thermionic current density is calculated from the Richardson-Dushmann equation[1,4,5] corrected for the Schottky effect.

2) Ion Flux Equation

The conservation of the ion flux imposes a balance between the ions formed by ionization and the ions crossing the boundaries of the control volume, Eq. (14).

$$\dot{n}_{ion}+\dot{n}_{in}=\dot{n}_{out} \tag{14}$$

$$q\pi r_e^2 L_{eff} n_o n K_i + j_{i,o}\pi r_o^2 = j_i\left(A_{eff}+\pi r_e^2-\pi r_o^2\right)+j_{th}\pi r_e^2 \tag{15}$$

In the Equation (14), $\dot{n}_{\mathrm{ion}}$ indicates the ion production rate due to direct electron-impact ionization, $\dot{n}_{\mathrm{in}}$ represents the contribution of the ions generated in the orifice and accelerated toward the insert as they cross the double sheath. $\dot{n}_{\mathrm{out}}$ includes the losses at the sheath boundaries as well as the thermal flux to the upstream section of the control volume, Eq. (15).

3) Internal Power Balance

Regarding the power balance, the model takes into account the plasma heating due to the Joule effect, P_R, the power delivered to the plasma by the ions arriving from the orifice, $P_{i,o}$, and the power gained by the emitted electrons, P_{em}. The contributions to plasma cooling are tied with the power removed by the ions leaving the control volume, P_i, the loss due to the electrons recombining on the emitter surface, P_{er} and the convection by the electron current, P_{conv}, as highlighted in the following expression, Eq. (16-17).

$$P_{i,O}+P_R+P_{em}=P_i+P_{er}+P_{conv} \tag{16}$$

$$j_{i,o}\left(V_{ds}+2\frac{k_B T_s}{q}\right)\pi r_o^2+RI_d^2+j_{em}\left(V_p+\frac{3}{2}\frac{k_B T_s}{q}\right)A_{eff} = \dot{n}_{out}\left(\langle\varepsilon_i\rangle+2\frac{k_B T_s}{q}\right)+j_{er}2\frac{k_B T_s}{q}A_{eff}+\frac{5}{2}\frac{k_B T_e}{q}I_d \tag{17}$$

4) Pressure Equation

The last equation has been obtained by balancing the plasma pressure in the emitter region, as given by the kinetic theory, and the pressure at the downstream end of the control volume. The gasdynamic derivation follows the work of Domonkos[5], which considers a Poiseuille flow with a linearized pressure gradient in the orifice region. The pressure balance results:

$$P_{kin} = P_{cont} \tag{18}$$

$$(n_{e,e} + n_{0,e})k_B T_s\left(1 + \frac{\alpha T_e}{T_s}\right) = \sqrt{\frac{\dot{m}128\,\mu}{\pi r_o^2} R_g T_{w,o} 2L_o + P_o^2} + \frac{1}{2}\left(\frac{P_o}{R_g T_{w,o}}\right)\bar{u}_o^2\,(1 + K_l) \tag{19}$$

Where:

$$\bar{u}_o^2 = \gamma R_g T_{w,o} \tag{20}$$

$$P_o = \frac{\dot{m} R_g T_{w,o} 4}{\pi d_o^2}\sqrt{\frac{1}{R_g \gamma T_{w,o}}} \tag{21}$$

In order to calculate the dynamic viscosity we use the Equation (22), according to Ref.1.

$$\mu = 2.3 \cdot 10^{-5} \cdot T_r^{0.71 + \frac{0.29}{T_r}} \quad , \quad T_r = T_{w,o}/289.7 \tag{22}$$

D. Thermal model

Calculation of the temperature within the components of a hollow cathode is crucial, particularly for low power applications. The design must guarantee the right thermal distribution, which does not compromise cathode functioning: too high temperature would cause heat dissipation problem, on the other hand, too low temperature would turn off thermionic emission. Thermal gradients must be also get under control, in order to avoid high thermal stresses.

A Lumped Elements Thermal Model[10], named LETherM, has been developed in the present work to quickly compute the temperature profile along the cathode axis, and more particularly the insert and orifice temperatures (used in the plasma model). The cathode is subdivided into few elements (Figure 4) with the purpose of getting a simple thermal network (Figure 5), where each node refers to a specific element.

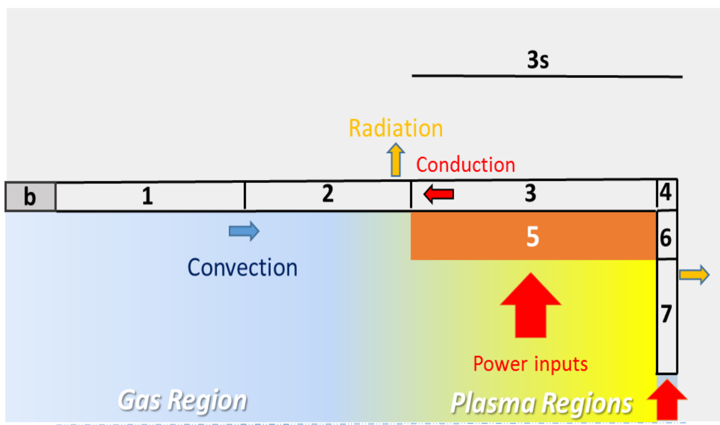

Figure 4. Schematic of the cathode with thermal shield and without keeper.

Perfect contact conditions are assumed among the cathode elements and the thermal deformations are neglected thus considering constant areas for heat exchanges. The thermal model includes temperature dependent expressions for the thermal conductivity of the materials and for the surfaces' emissivity as found in literature.

Regarding the heat transfer due to radiation, the surfaces are considered opaque, grey and isothermal with uniform radiation contributions. The view factor between the insert and the part of the orifice plate facing the interior of the cathode is computed following Howell[11], while the view factors of the external surface of the tube toward the vacuum chamber are taken equal to one. Neglecting the amount of radiation escaping from the ends of the heat shield, the view factor between the facing node of the tube and the shield is approximated to one.

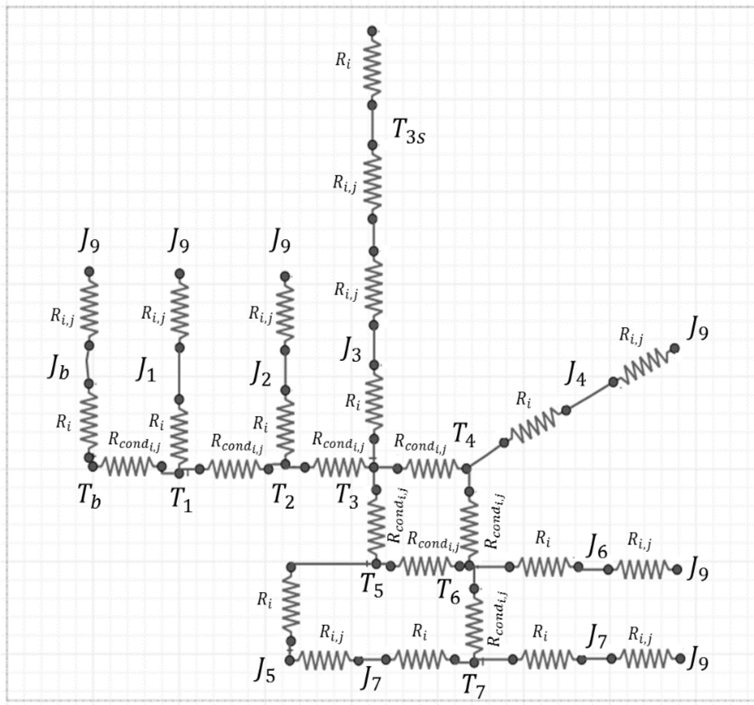

Figure 5. Thermal network of the cathode without keeper

A Matlab® routine solves iteratively the set of equations to compute the temperature of each node. Two types of equations form the system. The first type is identified by the blackbody emissive power and, consequently, by the temperature. The corresponding power balance writes:

$$-P_{in} + \frac{(\sigma_{SB} T_i^4 - J_i)}{R_i} + \frac{\sum_j (T_i - T_j)}{R_{cond_{i,j}}} = 0 \tag{28}$$

where P_{in} stands for the external power input to node i. Particularly the emitter is heated by the ions recombining on the wall and the back-streaming electrons, while is cooled by the emitted thermionic electrons leaving the surface whereas the ohmic power, as computed in the orifice model, is assumed to be completely transferred to the orifice wall. The power balance of the node representing the insert includes the loss by evaporation, too. The convective heat transfer is included in the model where nodes are in contact with gas.

For the second kind of node, indicated by the respective radiosity, J_i, the power balance is expressed as:

$$\sum_j \frac{(J_i - J_j)}{R_{i,j}} - \frac{(\sigma_{SB} T_i^4 - J_i)}{R_i} = 0 \tag{29}$$

The temperature of the cathode base element is kept at a constant value.

Keeper is not modelled. This simplification affects slightly the calculation concerning high power hollow cathodes but it led to underestimated temperatures, dealing with low power applications: Finite Element Method (FEM) simulations, not reported here for the sake of brevity, have shown a temperature increase of 100 K within the insert with keeper. The FEM model has been adopted to validate LETherM results, too.

Finally, it is worth to notice that LETherM is suitable only for a preliminary design phase. In a detailed design phase, 3D FEM model is more appropriate to analyse the whole cathode configuration.

IV. Results

In order to be confident with the results computed by means of the developed models, several test cases have been selected. In order to simplify the verifications, at first, the models have been tested separately. Four low current xenon cathodes [1,5,12,13,] using different insert material, have been selected to validate insert and orifice plasma modules.

Dealing with the thermal model, temperature and heat flux distributions along a reference cathode geometry[1], have compared to both literature data and the FEM model results.

A. Plasma Models

Table 1 summarizes the test cases selected to validate plasma modules implemented in the tool described above. At first, orifice and insert plasma models have been tested alone[12,13] (case number 1 and 2, respectively) and the results of the analyses have been compared to those available in literature [3,4,5,13,14,15,16,17,18]. Then they have been coupled[1,5] (test case 3 and 4), as described previously.

It is worth to notice that the validation phase deals with cathodes using Xenon as working fluid and low power discharge current (less than 3 A).

Table 1. Plasma Models' Validation Test Cases.

TEST CASE ID	1	2	3	4
Reference	**NSTAR[12]**	**Wilbur[13]**	**Domonkos[5]**	**Pedrini[3]**
Plasma Region	***Orifice***	***Insert***	***Orifice + Insert***	***Orifice + Insert***
Available data	***Num.***	***Exp./Num.***	***Num.***	***Num.***
Insert internal diameter [mm]	3.8	3.8	1.22	3
Orifice length [mm]	0.75	1.22	0.71	0.36
Orifice Diameter [mm]	0.28	0.76	0.15	0.4
Mass flow rate [mg/s]	0.36	0.127	[0.11 ÷ 0.23]	[0.3 ÷ 2]
Discharge Current [A]	3.26	[1.24 ÷ 4.26]	[0.75 ÷ 1.25]	[1 ÷ 3]
Insert Material	*Ba*	*(Ba/Sr)* CO_3	*W-BaO-CaO-*Al_3O_3	LaB_6

Dealing with test case 1, Table 2 reports the plasma densities and the electron temperature computed in the present study compared to those presented in literature. The electron temperature and the number density are close to Albertoni[4] and Korkmaz[14] computations (the error is less than 10%).

With respect to 0-D models' computations by Korkmaz[14] the neutral density is under predicted, but it is in good agreement with that of Albertoni[4].

There is higher electron temperature along with lower plasma and neutral densities with respect to the predictions of the 0-D model by Mizrahi[15], and the 0-D model by Mandell and Katz[16] (this two models include the energy loss due to excitation events in the plasma energy balance, neglected in the present study). Finally, there is a good agreement with the values predicted by the 2-D model of Mikellides and Katz[17] at the orifice outlet.

Concerning the test case number 2, Figure 6 shows the plots of the electron number density and plasma potential as function of discharge current, within the insert region of Wilbur's cathode[13]. It can be noticed that the model follows the experimental data trend where electron number density increases with the discharge current. Furthermore, the model well predicts that the emitter sheath voltage drop function has a relative minimum value at discharge current of 2.3 A (trend not detected by Wilbur's model). The present study's calculations over predict the electron number density by about 30% and under predict the sheath voltage drop by 18%, with respect to experimental data.

Table 2. NSTAR cathode: comparison of orifice plasma parameters.

Model reference	**0-D Present study**	0-D Mizrahi[15]	0-D Mandell and Katz[16]	0-D Korkmaz and Celik[14]	0-D Albertoni et al.[4]	1-D Katz et al.[18]			2-D Mikellides and Katz[17]		
Plasma parameter	**Average**	Average	Average	Average	Average	Orifice inlet	Maximum reached value	Orifice outlet	Orifice inlet	Maximum reached value	Orifice outlet
$n_{0,o}$, 10^{23} m^{-3}	**0.15**	1.1	0.4	0.6	0.2	2.8	2.8	0.6	0.65	0.65	0.1
$n_{e,o}$, 10^{22} m^{-3}	**0.77**	2.7	1	0.7	0.7	2.8	6	1.8	2	2.2	0.5
$T_{e,o}$, eV	**2.45**	1.6	2.2	2.4	2.7	1.2	1.8	1.8	2	2.2	2.2
$n_{e,o}/(n_{e,o}+n_{0,o})$	**0.34**	0.2	0.18	0.1	0.24	0.09	0.24	0.23	0.23	0.5	0.33

The emitter wall temperature and effective emission length as function of the discharge current are reported in Figure 7.

The emission length increases with the discharge current and the values lays within the experimental data, being in good agreement with respect to Wilbur model computations, too. On the contrary, the present model does not predict the emitter temperature increase with discharge current, but it matches the average value.

This is an indirect crosscheck to verify the errors of the present model's results with respect to the those of Wilbur: the effective emission length and the insert wall temperature are output of Wilbur model, whereas they are input of the model here presented.

Analyzing the results of test case 3, Figure 8, several considerations can be deduced. According to Domonkos numerical results[5], plasma densities increase with the discharge current and mass flow rate, even if the present model predict higher rate of orifice electron number density as function of mass flow rate. The electron number density is over predicted at most by 50% with respect Domonkos model[5] calculations.

There is a good agreement for both orifice and insert plasma electron temperatures (affected by a maximum error of about 3% in terms of Kelvin degrees). It is interesting to note that the electron temperature within orifice region changes with discharge current (trend not detected by Domonkos model[5]).

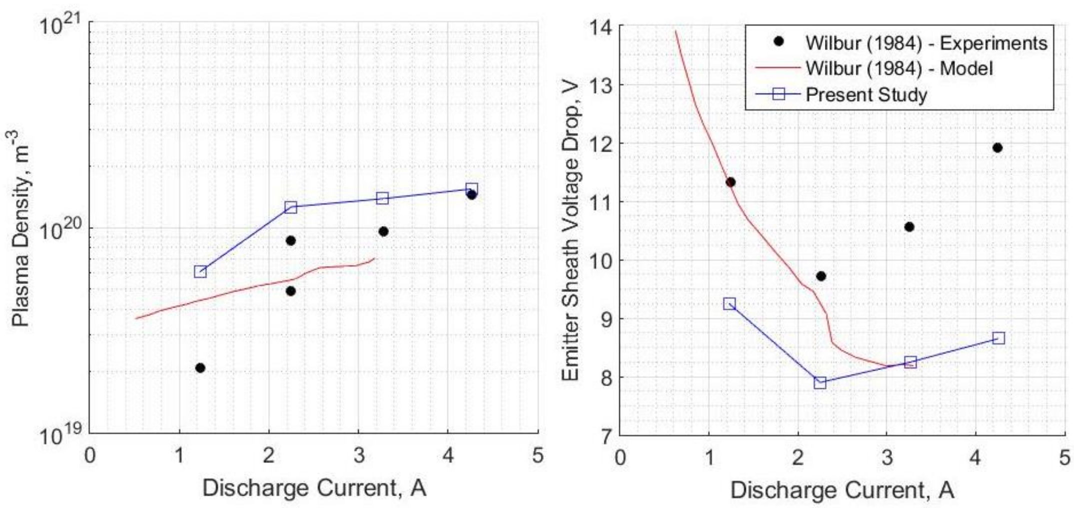

a) b)

Figure 6. Wilbur cathode[13]: insert plasma density (a) and emitter sheath voltage drop (b) as function of discharge current.

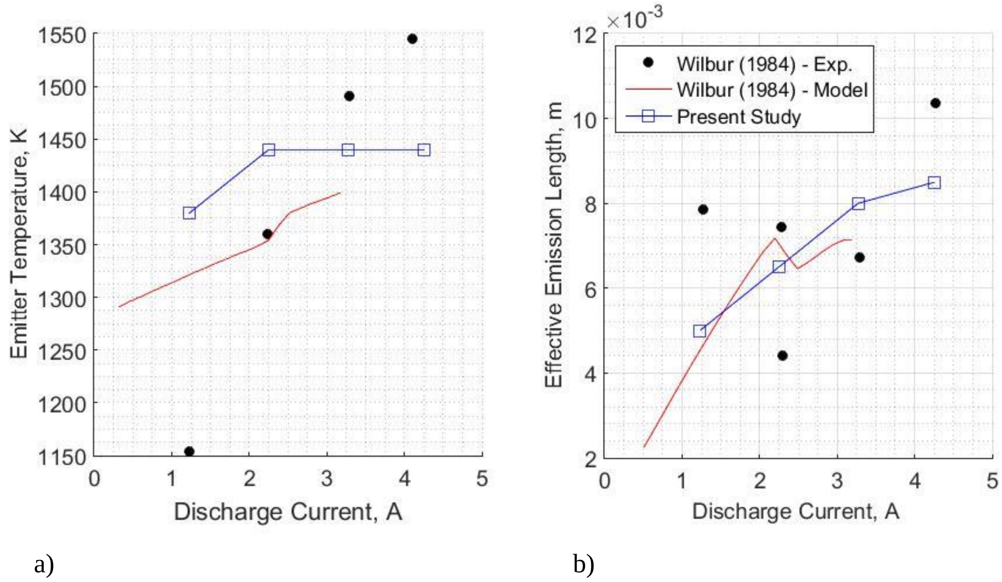

Figure 7. Wilbur cathode[13]: emitter temperature (a) and effective emission length (b) as function of discharge current.

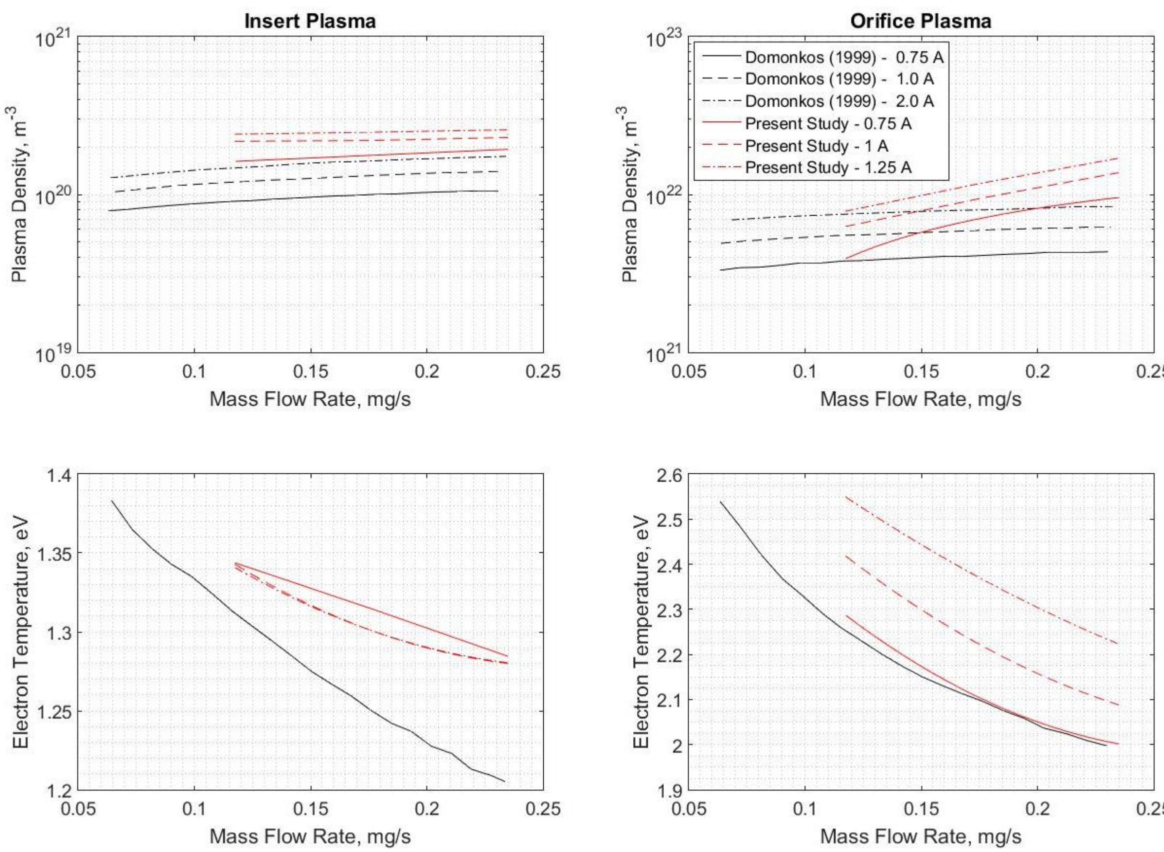

Figure 8. Domonkos cathode[5]: electron number density and electron temperature of insert and orifice plasmas as function of mass flow rate varying the discharge current.

B. Thermal Model

The baseline OHC geometry selected for a *code-to-code* comparison is the one proposed by Pedrini et al.[3]. It is mainly composed by a tantalum tube, about 20 mm long, using LaB_6 insert, the internal diameter of which is 3 mm. The orifice diameter is 0.4 mm. A tantalum thick foil wraps the main tube with the function of heat shield. The cathode operates at a discharge current of 3A and at mass flow rates of 0.3 mg/s of Xenon.

Temperature distributions along the cathode, reported in Ref. 3 and computed by LETherM and by FEM models, are shown in Figure 9a, Figure 10, and Figure 11, respectively.

The values predicted from LETherM (Figure 10) are marginally lower than those computed in Ref. 3 (Figure 9a) and are quite in a good agreement with those computed by FEM model, particularly in the emitter node (number 5, Figure 4) and those surrounding it (node numbers: 3, 4, 6).

Slight differences between LETherM and FEM model could be observed in the orifice region, where FEM model predicts a value of 1807 K that is closer to the reference value of 1802 K.

Quantitatively, the difference between LETherM results and reference temperatures, in the worst case, is 8% (node 2) and 7% (heat shield node) but it shrinks to less than 4% in remaining nodes.

The highest temperature difference could be noticed in node 2, it depends mainly on the calculated conduction and radiation powers. Indeed, LETherM predicts 12 W leaving the external surface of the cathode tube and about 11 W via conduction (Figure 10) against, respectively, 7 W and 16 W declared in the reference calculation (Figure 9b). The reason is the different selection of base material (more conductive; indeed Pedini et al.[3] did not declare the base material) or a local reduction of emissivity of the tube material.

The input power at the emitter node is function of its own temperature, because the thermionic electron emission: and this could explain the difference between the LETherM calculation (25.2 W, Figure 10) and the reference value (22.7, Figure 9b). In order to conclude, it can be said that LETherM under predicts the temperature distribution by an error less than 8% with respect to FEM or Pedrini[3] calculations.

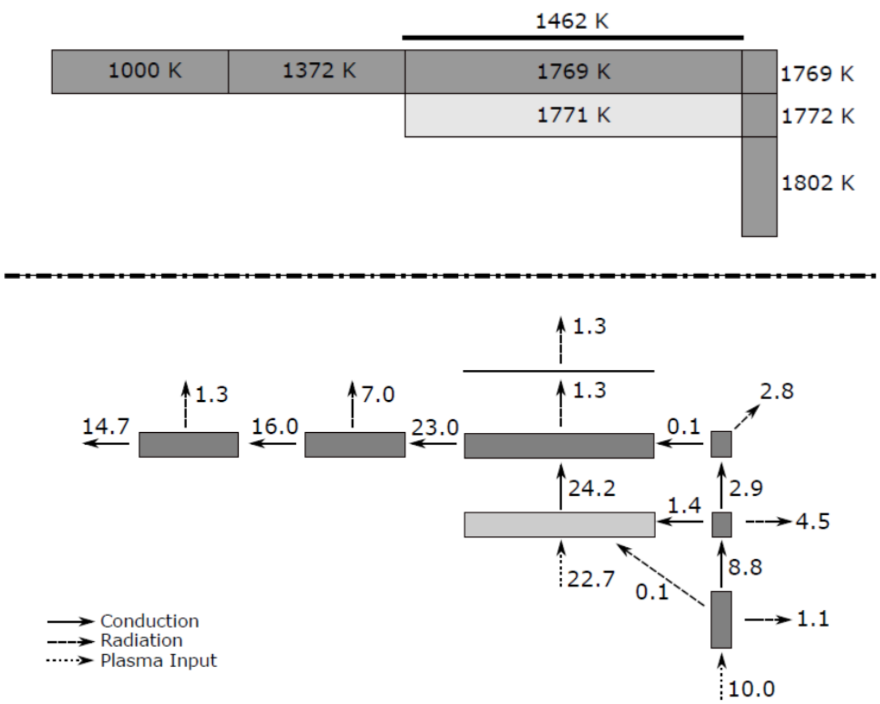

a)

b)

Figure 9. (a) Temperature [K] and (b) power distributions [W] along the cathode (Ref. 3).

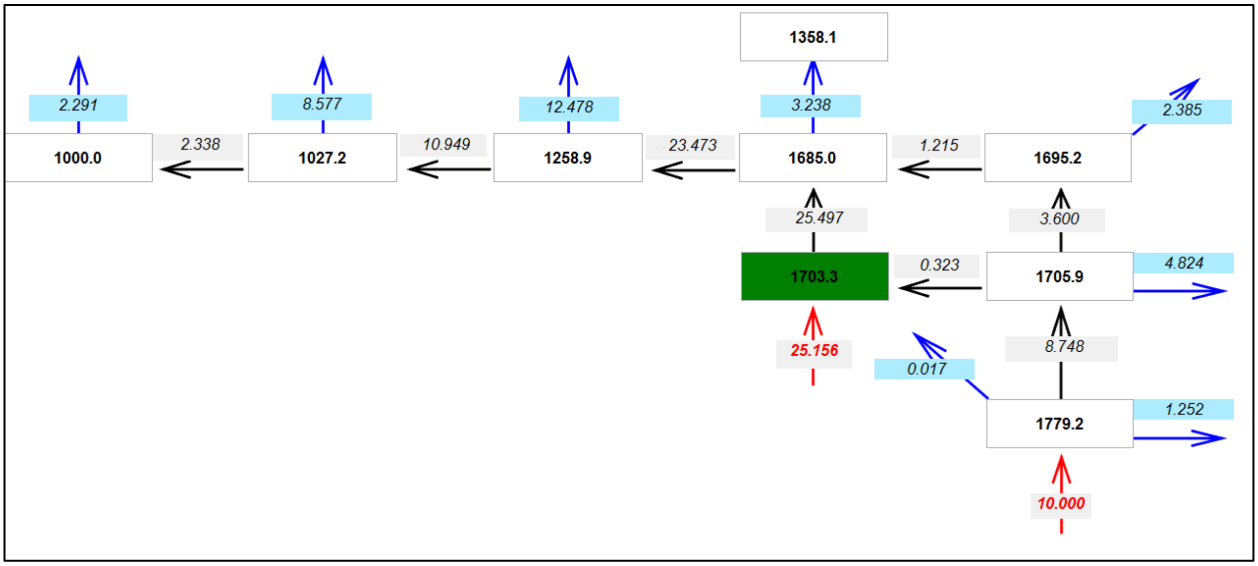

Figure 10. Temperature [K] and power distributions [W] along the cathode (by LETherM).

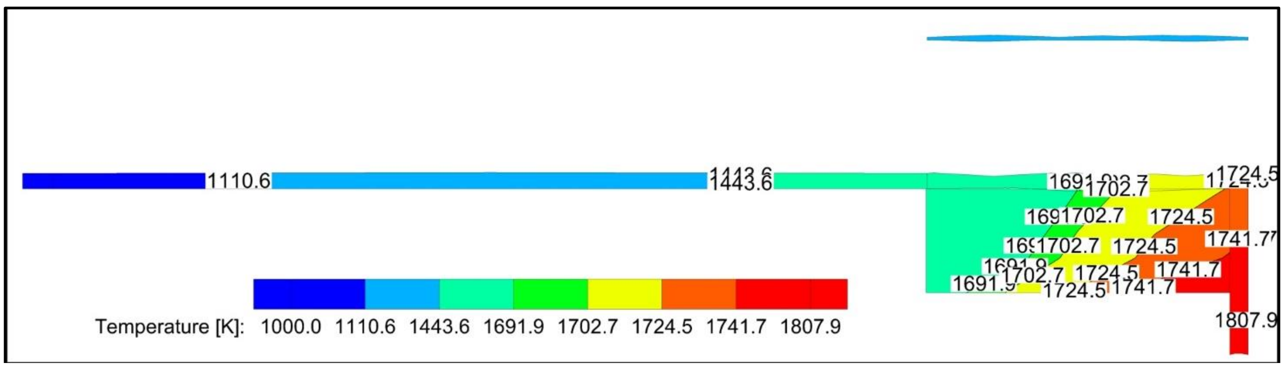

Figure 11. Temperature distributions [K] along the cathode (by FEM model).

V. Conclusion

A numerical tool, that simulates physical behavior of orificed hollow cathodes with low work function inserts, combining relevant literature models, has been developed and preliminary validated with available literature data.

Future work on numerical tool foresees the validation of plasma-thermal model coupling and the introduction of keeper, which implies the modification of thermal model and the evaluation of plasma parameters in the cathode-to-keeper region. Tool results could be used in order to define design guidelines for new cathodes, and in particular the tool has been used to design CIRA cathode for low power thrusters to be tested in the forthcoming CIRA facility MSVC. The cathode will be used for the final validation of the model.

Acknowledgments

The authors want to thank Valeria De Simone (Thermal structures and Design unit at CIRA) for the support in the FEM cathode simulation and all people involved in CIRA IMP-EP project.

References

[1]Goebel, D. M., and Katz, I., Fundamentals of Electric Propulsion: Ion and Hall Thrusters, John Wiley and Sons, NJ 2008.

[2] Paganucci, F., Pedrini, D. and Becatti, G. "Development of Hollow Cathodes for Electric Thrusters: Theoretical and Experimental Results", *International Workshop Ion Propulsion and Accelerator Industrial Applications IPAIA,* Bari, Italy, March, 2017.

[3]Pedrini, D. Albertoni, R. and Paganucci, F. "Theoretical Model of a Lanthanum Hexaboride Hollow Cathode," *33rd International Electric Propulsion Conference*", Washington, D.C., USA, 2013.

[4]Albertoni, R., Pedrini, D., Paganucci, F. and Andrenucci, M., "A Reduced-Order Model for Thermionic Hollow Cathodes," *IEEE Trans. Plasma Sci.*, vol. 41, No. 7, 2013, pp. 1731-1745.

[5]Domonkos, M. T. , "Evaluation of Low-Current Orificed Hollow Cathodes", PhD dissertation, Dept. Aerosp. Eng., Univ. Michigan, Ann Arbor, MI, USA, 1999.

[6]Chang, C. H. and Pfender, E., "Non equilibrium modeling of low-pressure argon plasma jets; Part I: Laminar flow", *Plasma Chemistry and Plasma Processing*, Vol. 10, No. 3, 1990, pp. 473-491.

[7]Capacci, M., Minucci, M., and Severi, A., "A simple numerical model describing discharge parameters in orificed hollow cathode devices", *33rd Joint Propulsion Conference and Exhibit*, Seattle, WA, 1997.

[8]Mandell, M. and Katz, I., "Theory of Hollow Cathode Operation in Spot and Plume Modes," *30th Joint Propulsion Conference and Exhibit*, Indianapolis, U.S.A., 1994.

[9]Siegfried, D. E., and Wilbur, P. J., "An investigation of mercury hollow cathode phenomena," *13th Int. Electr. Propuls. Conf.*, San Diego, CA, USA, Apr. 1978.

[10]Incropera, F. P., DeWitt, D. P., Bergman, T. L. , and Lavine, A. S., *Fundamentals of Heat and Mass Transfer*, Wiley, New York, NY, USA, 2006.

[11]Howell, J. R., and Siegel, R., *Thermal Radiation Heat Transfer*, 5th ed. Boca Raton, FL, USA, 2010.

[12]Goebel, D. M., Watkins, R. M., and Jameson, K. K., "LaB6 Hollow Cathodes for Ion and Hall Thrusters," *Journal of Propulsion and Power*, vol. 23, No. 3, 2007, pp.552–558.

[13]Wilbur, P. J., "Advanced Ion Thruster Research Annual Report, I", NASA CR-168340, 1984.

[14]Korkmaz, O., and Celik, M., "Global Numerical Model for the Assessment of the Effect of Geometry and Operation Conditions on Insert and Orifice Region Plasmas of a Thermionic Hollow Cathode Electron Source," *Contrib. Plasma Phys.*, vol 54, No. 10, 2014, pp. 838 – 850.

[15]Mizrahi, J., Vekselman, V., Gurovich, V. and Krasik, Y.E., "Simulation of plasma parameters during hollow cathodes operation," *Journal of Propulsion and Power*, vol 28, No. 5, 2012, pp. 1134.

[16]Mandell, M. and Katz, I., "Theory of Hollow Cathode Operation in Spot and Plume Modes," *30th Joint Propulsion Conference and Exhibit*, Indianapolis, U.S.A., 1994.

[17]Mikellides, I., and Katz, I., "Wear Mechanisms in Electron Sources for Ion Propulsion, 1: Neutralizer Hollow Cathode," *Journal of Propulsion and Power*, vol. 24, No. 4, 2008, pp. 855–865.

[18]Katz, I., Anderson, J.R., Polk, J. E. and Brophy, J. R., "One-Dimensional Hollow Cathode Model," *Journal of Propulsion and Power*, vol. 19, No. 4, 2003, pp. 595–600.